Biomed Microdevices (2008) 10:899–908
DOI 10.1007/s10544-008-9204-5

Design optimization for bioMEMS studies of enzyme-controlled metabolic pathways

Xiaolong Luo · Dean Larios Berlin · Susan Buckhout-White · William E. Bentley · Gregory F. Payne · Reza Ghodssi · Gary W. Rubloff

Published online: 15 July 2008

Abstract Biological microelectromechanical systems (bioMEMS) provide an attractive approach to understanding and modifying enzymatic pathways by separating and interrogating individual reaction steps at localized sites in a microfluidic network. We have previously shown that electrodeposited chitosan enables immobilization of an enzyme at a specific site while maintaining its catalytic activity. While promising as a methodology to replicate metabolic pathways and search for inhibitors as drug candidates, these investigations also revealed unintended (or parasitic) effects, including products generated by the enzyme either (1) in the homogeneous phase (in the liquid), or (2) nonspecifically bound to microchannel surfaces. Here we report on bioMEMS designs which significantly suppress these parasitic effects. To reduce homogeneous reactions we have developed a new packaging and assembly strategy which eliminates fluid reservoirs that are commonly used for fluidic interconnects with external tubing. To suppress reactions by nonspecifically bound enzyme on microchannel walls we have implemented a cross-flow microfluidic network design so that enzyme flow for assembly and substrate/product for reaction share only the region where the enzyme is immobilized at the intended reaction site. Our results show that the signal-to-background ratio of sequential enzymatic reactions increases from 0.72 to 1.28 by eliminating the packaging reservoirs, and increases to 2.43 by separating the flow direction of enzymatic reaction from that of enzyme assembly step. These techniques can be easily applied to versatile microfluidic devices to minimize parasitic reactions in sequential biochemical reactions.

Keywords Parasitic reaction · Enzyme immobilization · Non-specific binding · Dead-volume · Cross-channel design · Packaging aligner

Electronic supplementary material The online version of this article (doi:10.1007/s10544-008-9204-5) contains supplementary material, which is available to authorized users.

X. Luo · D. Larios Berlin · W. E. Bentley
Fischell Department of Bioengineering, University of Maryland, College Park, MD 20742, USA

X. Luo · D. Larios Berlin · S. Buckhout-White · G. W. Rubloff
Institute for Systems Research (ISR), University of Maryland, College Park, MD 20742, USA

W. E. Bentley · G. F. Payne
University of Maryland Biotechnology Institute (UMBI), University of Maryland, College Park, MD 20742, USA

R. Ghodssi
Department of Electrical and Computer Engineering, University of Maryland, College Park, MD 20742, USA

S. Buckhout-White · R. Ghodssi · G. W. Rubloff (✉)
Department of Materials Science and Engineering, University of Maryland, College Park, MD 20742, USA
e-mail: rubloff@umd.edu

1 Introduction

1.1 Motivation: enzymatic reactions and metabolic pathways in bioMEMS

Microfluidic devices and polydimethylsiloxane (PDMS) soft lithography fabrication have reduced the size, reagent quantity, and cost of many standard biochemical analytical protocols, by handling nanoliter volumes (Janasek et al. 2006, Quake and Scherer 2000). Biological

micro-electromechanical systems (bioMEMS) are an important subset of these devices that are able to recreate biomolecular reaction pathways. Of particular interest are pathways that play a critical role in the functionality and behavior of living cells. Enzyme catalysis is central to many of these pathways, and accordingly it has been a major goal to develop means to isolate enzymes at specific locations in a microfluidic system, and confirm that their catalytic action is maintained in this artificial setting. This would provide an attractive testbed for understanding the details of reaction pathways and kinetics, and for identifying means to modify pathways (e.g., for discovery of a drug that can significantly suppress, enhance, or modify the dominant pathway).

Our group has demonstrated bioMEMS technology that enables the programmable assembly of biomolecules on localized assembly sites in microchannels (Park et al. 2006) using electrodeposition of the amine-rich polysaccharide chitosan to direct the assembly (Wu et al. 2003, Yi et al. 2005). We recently demonstrated that a metabolic pathway enzyme, *S*-adenosylhomocysteine nucleosidase (Pfs), can be assembled in this way and that its catalytic action is retained in the microfluidic environment, shown by conversion of substrate *S*-adenosylhomocysteine (SAH) into products *S*-ribosylhomocysteine (SRH) and adenine, as illustrated in Fig. 1(a)–(c) (Luo et al. 2008). This reaction step is known to be one of two enzyme reaction steps by which bacteria produce autoinducer-2 (AI-2), a small cell-signaling molecule that serves as a quorum-sensing communicator, through which bacterial populations exhibit altered phenotype. Our ultimate goal is to use the bioMEMS environment as a testbed for discovery of molecules that inhibit quorum sensing. These would be good candidates for a new type of antimicrobial drug that would work by interfering with bacterial communication rather than by killing bacteria, hopefully avoiding drug-resistant mutations that are too often generated by direct attack on the bacteria.

1.2 Limitations and goals

While these results showed clear enzyme activity at the assembled active sites, it was accompanied by notable (approximately 15–30%) background (or "parasitic") reac-

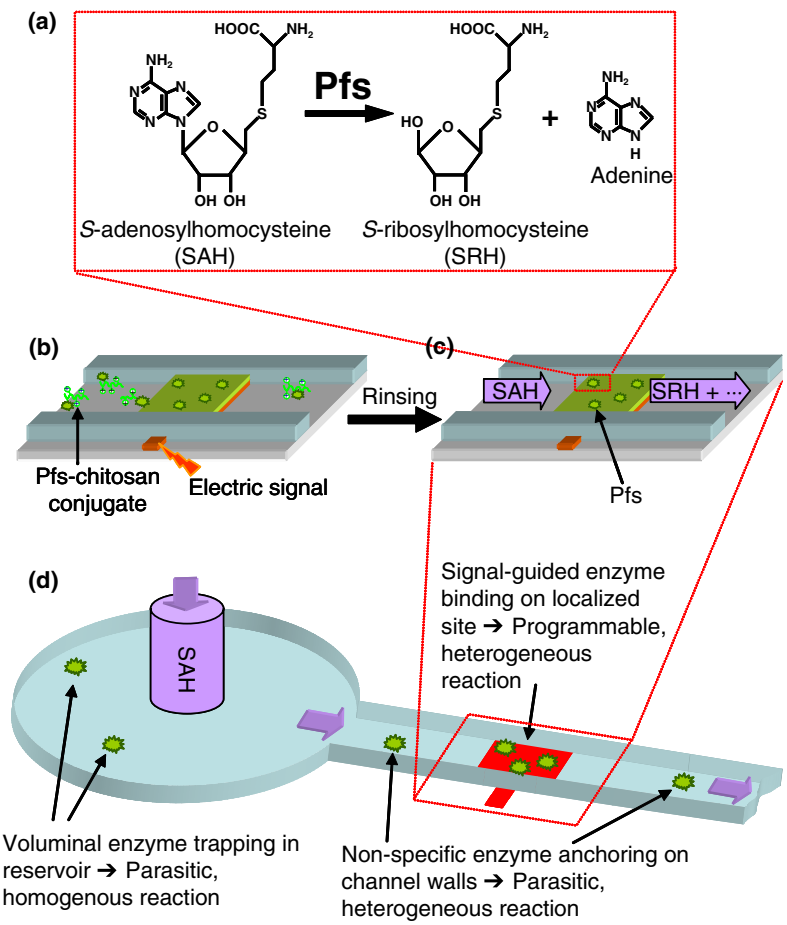

Fig. 1 Parasitic reactions in microfluidics due to enzyme trapped in interconnect reservoirs and non-specifically bound on microchannel walls. (**a**) Pfs enzyme converts SAH substrate into products SRH and adenine. (**b**) Electrical signal-guided assembly of Pfs-chitosan conjugate onto a localized assembly electrode in a microchannel followed by buffer rinsing. (**c**) Sequential enzymatic reaction in continuous flow in the microchannel. (**d**) Parasitic reactions in reservoirs and on microchannel wall as well as programmable reactions on localized enzyme assembly site

tion that occurred elsewhere in the microfluidic system (signal/background ratio, or S/B, =3−6×). This is not surprising, given that the surface area and volume at the reaction site comprised only ~0.2% of the total wall area and volume of the microfluidic system. The result indicates that the active site is >1,000× more efficient than unintended (parasitic) sites in the microfluidic network. These background signals appear in control experiments and are not associated with the intended catalytic action at the enzyme assembly sites. Accordingly we refer to these background reaction channels as "parasitic" in that they produce reactions that add to and interfere with efforts to localize reactions at the electrode sites.

The purpose of the present work is to reduce two significant parasitic reaction mechanisms in our bioMEMS. One is a homogeneous reaction mechanism, in that substrate and enzyme react while in the fluid phase. It occurs because active enzyme is retained in reservoir areas where fluidic interconnects are made at the packaging level. The other is a heterogeneous reaction mechanism, in which enzyme nonspecifically bound to microfluidic channel walls reacts with substrate impinging from the fluid phase. These mechanisms are depicted schematically in Fig. 1(d).

1.3 Eliminating reservoir dead volume

Connections between a bioMEMS device and external sources of fluids are essential to operate the device. However, alignment of fluidic inputs/outputs (I/Os) to the microchannels can be challenging. A conventional approach is to design a larger fluidic reservoir as an interface between on-chip microfluidic channels and external fluidic connections at the packaging level, reducing the precision needed for alignment. This approach has been used for tubing connection in microfluidics from individual microsystems (Bilitewski et al. 2003, Han et al. 2005, Kim et al. 2007, Long et al. 2007) to large-scale integration (McDonald and Whitesides 2002, Thorsen et al. 2002, Urban et al. 2006). The reservoirs are not readily flushed since their geometry leaves dead volume regions which entrap reactive biomolecules (e.g. enzymes) for extended periods of time, causing homogeneous parasitic reactions and altering the apparent conversion efficiency and time dependence of intended enzyme reaction steps (Ku et al. 2006, Luo et al. 2008).

To avoid the homogenous parasitic reactions in interconnect dead volume, we implement a new packaging technique that involves fabricating aligners on soft lithography molds to improve the alignment capability for interfacing between in-plane microfluidic channels and external tubing. The macro-scale packaging and assembly technology issues and their effect on microfluidic performance have been reviewed in literature (Fredrickson and Fan 2004). Our design eliminates the interconnect reservoirs by fabricating on-chip SU-8 aligner plugs, analogous to Si plugs made by DRIE (Gray et al. 2004), to guide microfluidic packaging connections. The relevant properties of PDMS which enable this technique are given elsewhere (McDonald and Whitesides 2002). Here we show PDMS sealing around tubing 20% larger than the nominal hole diameter, building on the demonstration in the literature (Christensen et al. 2005). We employ two rigid Plexiglas plates to clamp the PDMS-glass device, and stabilize the pogo pins on their electrode contacts, similar to the demonstration by Bhagat et al. (2007) where rigid clamps were employed to mechanically stabilize the tubing. We demonstrate that background biochemical activity is reduced by 33% in the new design.

1.4 Reducing impact of nonspecifically bound enzyme

The presence of microfluidic channel walls with area far in excess of that of the intended enzyme reaction site is intrinsic to the geometry of bioMEMS. As indicated in Fig. 1(d), however, our bioMEMS design employed a single channel to (1) first activate the enzyme to react with chitosan, and then deliver the enzyme-chitosan conjugate to be immobilized on the assembly site by electrical signal, and (2) subsequently to transport substrate to the active site and product away from it to a downstream collection point. This configuration exposed substrate to nonspecifically bound enzyme through the full length of the channel prior to its collection.

To reduce the contribution of enzyme nonspecifically bound on channel walls, we have implemented a cross-flow bioMEMS channel design. The channel that carries the enzyme-chitosan conjugate for immobilization is orthogonal to a second channel that carries substrate and product downstream to an exhaust location for analysis of enzymatic conversion. Thus, substrate is exposed to enzyme only at the active site, suppressing the contribution of nonspecifically bound enzyme to measured conversions.

This experimental strategy utilizing cross-flow microchannels to separate flow directions for sequential biochemical reactions has been broadly used in DNA/protein separation (Long et al. 2007), droplet formation (Tan et al. 2006) and enzymatic reaction (Bilitewski et al. 2003), where the cross area is the focus point for sample manipulation or for reagent introduction. In this work, we spatially assemble metabolic enzyme Pfs at the intersection between two flow channels so that we can separate the flow direction for enzyme assembly from the subsequent flow direction for enzymatic reaction. This design enhancement is an important advance toward our goal of reconstructing multiple metabolic pathway enzymes. Spatially separating individual reaction steps in microfluidics allows for an

understanding of reaction details and testing of molecules that can modify pathways and kinetics. In drug discovery, for example, a molecular species which inhibits a bacterial signaling pathway enzyme can be a candidate for an antimicrobial drug whose action is to interfere with cell signaling or quorum sensing. By using a cross-flow design to separate flow directions, we significantly suppress non-specific heterogeneous reactions on microchannel walls and reduce the background signal by an additional 50%. Together, these bioMEMS design modifications result in a combined enhancement of 3.38× in the signal/background ratio (from 0.72 to 2.43).

2 Detailed device design, fabrication and packaging

For this work we have employed a soft lithography molding approach (McDonald and Whitesides 2002) to the fabrication of the bioMEMS, in contrast to our previous work on enzyme reactions in bioMEMS (Luo et al. 2008). This accelerates development and testing of the concept, while removes some of the benefits of our earlier design (Park et al. 2006).

2.1 Packaging aligners to eliminate interconnect reservoirs

To avoid homogeneous parasitic reaction in interconnect dead volume, minimal or no interconnect reservoir is desired. To achieve this goal, we designed and fabricated packaging aligners using a soft lithography molding process. As shown in Fig. 2(a), packaging aligners of 500 μm in diameter were patterned from a 200 μm-thick SU-8 layer on the top of the 150 μm-thick SU-8 mold layer used to define the 500 μm-wide microchannels. A design offset of 1.07% was applied in the photomask to accommodate the shrinkage ratio of PDMS (Lee and Lee 2008). Figure 3(a) shows the fabricated prototype mold with packaging aligners.

Three ways of PDMS curing and packaging have been explored to assemble the final device without interconnect reservoirs to external tubing. In Fig. 2(b), a sharpened coupler (fabricated in-house from a 25 ga coupler, 0.020 in. OD) was used to punch through the 3 mm-thick PDMS layer along the pits formed by the packaging aligners during the PDMS curing process. Holes for electrical contact (0.1 in. diameter) were also punched in the PDMS before the microchannel side was wetted with methanol and

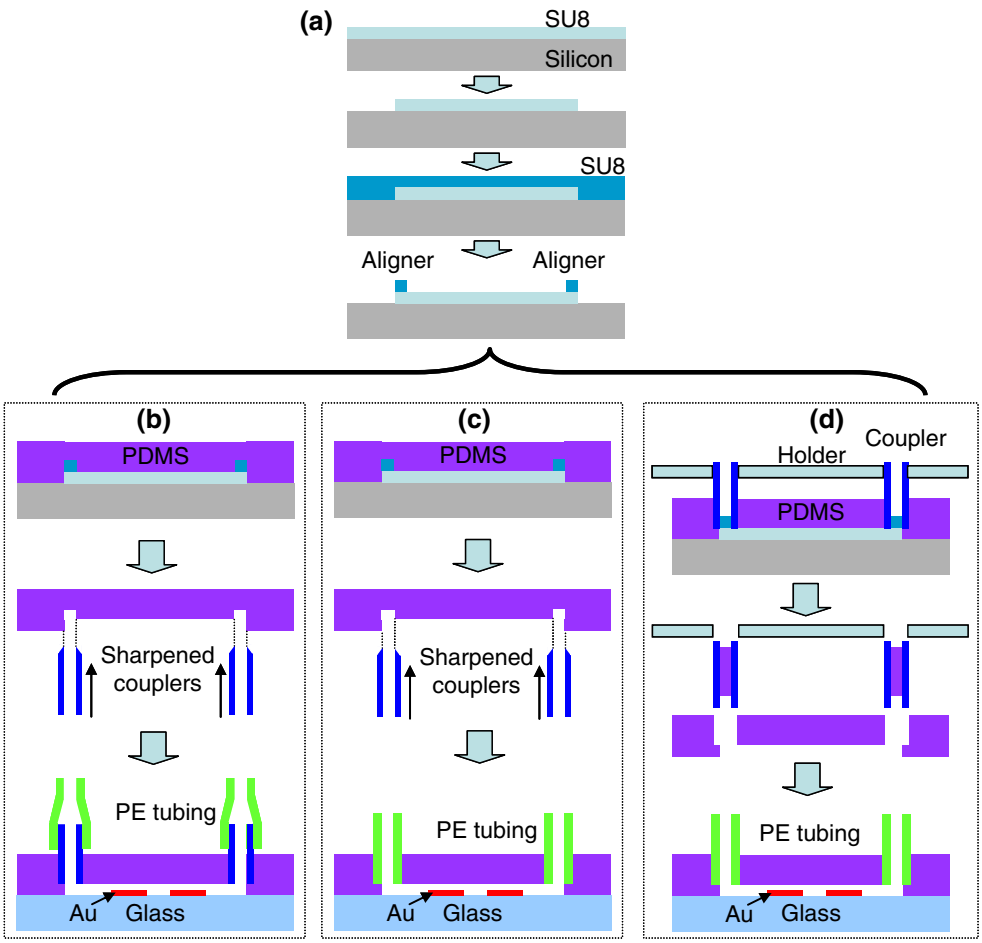

Fig. 2 Eliminating interconnect reservoirs by aligners on prototype mold to guide microfluidic packaging. (**a**) Aligners on prototype mold. (**b**) Packaging way #1: punch holes via PDMS followed by coupler insertion. (**c**) Packaging way #2: punch holes via PDMS followed by tubing insertion. (**d**) Packaging way #3: align couplers for PDMS curing followed by coupler removal and tubing insertion

bonded to a glass slide (2×1 in.). The whole device was then sandwiched with screws between two Plexiglas clamp plates, and with pogo pins inserted through holes in the top plate for electrical connection. Finally, flat-end couplers of the same size were inserted into the punched holes and connected to external PE tubing (0.015 in. ID).

Figure 2(c) shows the same strategy as Fig. 2(b) except that the external tubing was directly inserted into the punched holes in PDMS. In Fig. 2(d), couplers with inner-diameter of 0.024 in. (20ga, 0.036 in. OD) were gently placed onto the aligners of 0.5 mm OD and stabilized with a Plexiglas coupling holder while the PDMS cured. Then the couplers were removed and external microbore PTFE tubing (0.022 in. ID, 0.042 in. OD) was inserted into the well-defined connection holes (0.036 in. OD). Due to capillary action, couplers were normally filled with PDMS after curing, which was advantageous because it allowed a slug of PDMS to be removed, facilitating better sealing. A packaged device following the procedure of Fig. 2(d) is shown in Fig. 3(b) with blue dye flowing through the cross channel.

Finally, leak testing showed that all three strategies provide leak-tight sealing. The designs in Fig. 2(b) and (c) were predominantly used in our experiments since they minimized the dead volume between the coupler and tubing as well.

2.2 Cross-channel design to separate sequential flow directions

Cross channels (500 μm-wide, 150 μm-high) as shown in Fig. 3(b) were designed to separate the sequential flow direction of enzyme assembly (A→C) from the flow direction of the subsequent enzymatic reaction (B→D). No on-chip valves were included for this test-of-concept design. Parafilm was used to seal the connecting couplers/tubing that were not being used for a given experiment step to minimize the flow into these channels. After enzyme assembly, PBS buffer was pumped into the top three ports of the device in Fig. 3(b) to rinse the channels. In the following experiment, substrate was continuously pumped through the reaction site at the intersection for ~10 h. The serpentine channel connecting the bottom port was included to increase channel length in an efficient manner to prevent any enzyme from defusing back to the reaction site. The packaging aligners described above were also included for this cross-channel design.

3 Experimental methods

3.1 Materials

S-adenosylhomocysteine (SAH), bovine serum albumin (BSA), chitosan (minimum 85% deacetylated chitin; molecular weight 200,000 g/mol) from crab shells, imidazole, isopropyl β-D-thiogalactopyranoside (IPTG), nickel sulfate, phosphate buffered saline (PBS) (2.7 mM KCl, 137 mM NaCl, 1.5 mM KH_2PO_4, 8.1 mM Na_2HPO_4, pH 7.5), sodium cyanoborohydride, and tyrosinase from mushroom were purchased from Sigma (St. Louis, MO, USA). Tyrosinase was reported by the manufacturer to have an activity of 1,530 units/mg solid. LB (Luria broth) medium was purchased from Becton Dickinson (Cockeysville, MD, USA). Acetonitrile (HPLC grade), ampicillin sodium salt, chloroform, glycerol, sodium phosphate (monobasic), sodium phosphate (dibasic), and water (HPLC grade) were purchased from Fisher Chemical (Fair Lawn, NJ, USA). Hydrochloric acid and sodium chloride were purchased from J. T. Baker (Phillipsburg, NJ, USA). Non-fat dry milk

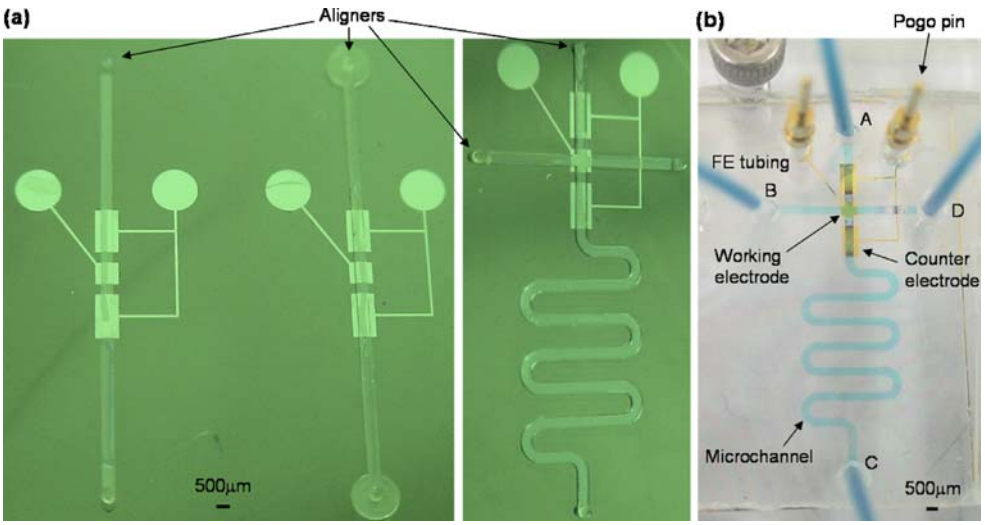

Fig. 3 Device and packaging. (**a**) Fabricated aligners on prototype mold. (**b**) Blue dye solution flowing through a packaged cross-channel without interconnect reservoirs. PE tubing was inserted. In experiment, enzyme solution flowed A→C, substrate solution flowed B→D

was purchased from BioRad (Hercules, CA, USA). Bleach was purchased from James Austin Co. (Mars, PA, USA). De-ionized water (ddH_2O, 18 MΩ·cm, Milli-Q) and PBS (dissolved in de-ionized water) were autoclaved before use.

Silicon wafers were purchased from University Wafer (South Boston, MA, USA). Plain and frosted micro slides, Single-Use Syringes/BD Needle Combinations, microcentrifuge tubes were purchased from VWR (West Chester, PA, USA). SU-8 photoresist was purchase from MicroChem (Newton, MA, USA). Sylgard® 184 silicone elastomer kit was purchased from Robert McKeown (Branchburg, NJ, USA). Steel couplers (25, 20 ga) and PE tubing were purchased from Instech Laboratories (Plymouth Meeting, PA, USA). Microbore PTFE tubing was purchased from ColeParmer (Vernon Hills, IL, USA). Genie Plus syringe pumps were purchased from Kent Scientific (Torrington, CT, USA).

3.2 Pfs-chitosan conjugate preparation

Chitosan, enzyme Pfs and Pfs-chitosan conjugate preparation procedures were reported elsewhere (Lewandowski et al. 2006, Luo et al. 2008). Briefly, Chitosan solution was prepared by dissolving chitosan flakes in HCl solution at pH ~2 overnight, then the pH was adjusted to pH 4.8 by adding 1 M NaOH dropwise before being filtered and stored at 4°C. Plasmid pTrcHis-Pfs-Tyr was first constructed by PCR amplification of *Pfs* from *E. coli* wild type strain W3110. Following digestion, the PCR products were extracted by gel purification and inserted into pTrcHisC (Invitrogen). DNA sequencing was performed to verify construct integrity. The plasmid was transformed into *E. coli* DH5α (defective *luxS* strain). *E. coli* DH5α containing pTrcHis-Pfs-Tyr was cultured and enzyme production was induced before the cells were lysed by sonication. Next, the enzyme was purified by ion-metal affinity chromatography (IMAC) before being mixed 2:1 with glycerol, divided into aliquots, and stored at −80°C. The conjugate was prepared by incubating enzyme Pfs, tyrosinase, and chitosan in sodium phosphate buffer for 2 h at room temperature followed by incubation in sodium cyanoborohydride for 30 min to stabilize Pfs-chitosan binding.

3.3 Enzyme assembly and enzymatic reactions

After leak-testing of the assembled microfluidic device, the microchannel and all the connecting tubing were rinsed with DI water at 50 μL/min flow rate for 30 min. Then, bovine serum albumin (BSA) solution (1% [*w*/*v*] in PBS buffer) was pumped into the microchannel at 3 μL/min flow rate for 2 h to block non-specific binding. After PBS buffer rinsing for 15 min at 5 μL/min flow rate, Pfs-chitosan conjugate solution was pumped at the same flow rate until the microchannel was completely filled before the pump was stopped. For all the control experiments to test the background signals, no electrical signal was applied to the working electrode during incubation of 240 s, as shown in Fig. 5. The Pfs-chitosan conjugate solution was then drained from the system, and the electrodeposited Pfs-chitosan conjugate was washed with PBS buffer at 5 μL/min flow rate for 30 min. Next, enzymatic reactions were performed by continuously pumping the SAH substrate solution (1 mM SAH in 50 mM sodium phosphate buffer, pH 7.2) for 2 h at 0.4, 1 and 4 μL/min flow rates by a Genie Plus syringe pump. During the second hour at each flow rate, samples were collected every 20 min. They were then extracted with chloroform and stored at −20°C before analyzing via HPLC.

For the experiments to test the overall conversion by site-specifically assembled enzyme and non-specifically assembled enzyme, an electrical signal of constant current density 3 A/m^2 was applied to maintain negative bias voltage on the working electrode for 240 s, while a second electrode served as the counter electrode. All other steps followed the same aforementioned procedure.

3.4 Analysis of enzymatic reaction products

A Waters Spherisorb Silica column (250×4.6 mm) with 5 μm beads (80 Å pore) was used in reversed-phase mode with 5 μL sample injection size and a mobile phase of 70:30 acetonitrile/water at 0.5 mL/min. The HPLC system consisted of two Dynamax model SD-200 pumps (with 10 ml pump heads and mixing valve) and a Dynamax Absorbance Detector model UV-D II, and data was analyzed using Star 5.5 Chromatography Software (Rainin). Conversion was calculated from elution data at 210 nm absorbance.

4 Quantification and simulation of interconnect dead volume

To better understand the degree to which interconnect dead volume affects the system response at a specific reaction site, we quantified and measured the changes in fluorescent dye intensity in the microchannel under flow, at a point 8.75 mm downstream of the interconnect point over the active electrode [Fig. 4(a)]. The interconnect reservoir is 2 mm in diameter and 0.15 mm high, and the microchannel is 0.5 mm wide. The upstream external tubing was first filled with dye solution (Cy5) before inserting into the PDMS device. The dye solution was pumped into the microchannel at 1 μL/min flow rate by a syringe pump, and a fluorescent microscope simultaneously recorded the dye intensity over the electrode. The microscope images were

converted into grayscale images and processed by Image J software (National Institutes of Health). As a comparison, quantification was also performed for a microchannel of the same dimension without the interconnect reservoir [Fig. 4(b)].

Figure 4(c) shows the changes in relative intensity over the electrode for a microchannel with interconnect reservoirs (pink solid line), and for a microchannel without interconnect reservoirs (blue dashed line). The left portion of the curves shows that it takes about 50 s for the dye solution to reach the electrode. The right portion of the curves shows that in the microchannel with the interconnect reservoir, the dye intensity increases from 10% to 90% in 61 s, while in the microchannel without interconnect reservoir it only takes 32 s. The intensity difference over time in the microchannels with and without reservoir [Fig. 4(e), blue line] differs for more than 100 s before it plateaus at the maximum value of 0.32.

Finite element simulation was also performed to investigate the effects of the interconnect reservoir on the system response at the same location as in the experimental quantification. This simulation was performed using COMSOL Multi-Physics by modeling the switching of the incoming flow to dye solution at the interconnection point, and by integrating the dye intensity over the electrode. The left portion of the simulation curves [Fig. 4(d)] shows that it also takes about 35 s for the dye solution to reach the electrode. The longer response time in this portion of the experiments is probably due the lag associated with pump startup and the extra tubing connecting the syringe pump. The right portion of the simulation curves shows that for a microchannel with an interconnect reservoir, it takes 75 s for the dye intensity to increase from 10% to 90% [Fig. 4(d), solid pink line], while for a microchannel without an interconnect reservoir it only takes 25 s [Fig. 4(d), dashed blue line]. The pink open line in Fig. 4(e) is the intensity difference in the microchannels with and without reservoir over time, which shows that the intensity over this specific electrode site differs for more than 100 s before it reaches plateau with the maximum value 0.30. The shorter time to reach plateau for the microchannel with reservoir in the experiments is probably because of the pump. The flow driven by our syringe pump is not strictly continuous, but advances in a step-wise manner that is disadvantageous in applications where smooth continuous flow is desired.

Together, both the experimental quantification and the finite element simulation confirm that the system response (as measured downstream at the reaction site) has improved 2~3 times by eliminating the dead volume in interconnect

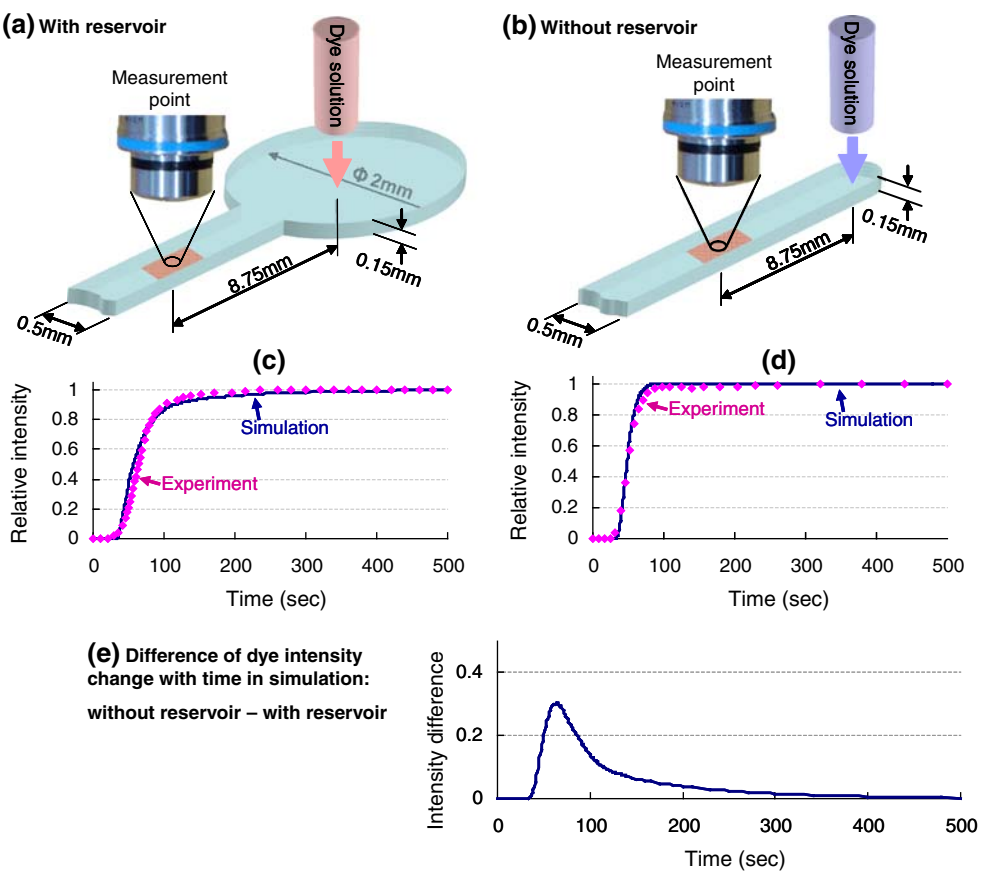

Fig. 4 Quantification and simulation of dye intensity change from the interconnect point. Dye intensity was monitored over electrode patches 12 mm downstream the microchannels. (**a**) Dye intensity change from interconnect with reservoir. (**b**) Dye intensity change from interconnect without reservoir. (**c**) Experimental quantification of dye intensity increasing from 10% to 90%: with reservoir, it takes 61 s; without reservoir, it takes 32 s. (**d**) Finite element simulation of dye intensity increasing from 10% to 90%: with reservoir, it takes 75 s; without reservoir, it takes 25 s. (**e**) The difference of intensity change from interconnects with and without reservoir

reservoirs, therefore avoiding the homogenous parasitic reactions in the dead volume.

5 Quantification of parasitic reactions and overall analysis

5.1 Enzyme reaction and controls

To determine the benefit of the design changes detailed above which focus on microfluidics, we compared enzymatic conversions in these various designs to test the effects of parasitic reactions. This is schematically indicated in Fig. 5 for the cases of (1) single channel with interconnect reservoirs, (2) single channel without interconnect reservoirs and (3) cross channel without reservoirs. The microchannels were first filled with Pfs enzyme solution, and then incubated in the enzyme solution in a static state for 4 min without applying an electrical signal to the assembly site (no electrodeposition). Next, enzyme solution was drained from the microchannel, and buffer solution was introduced to rinse the channel. Finally, enzymatic substrate SAH was introduced and the downstream solution was collected for analysis by HPLC.

The experimental results in Fig. 6 show that in the case of the single channel with reservoirs, the conversion of SAH into SRH and adenine was 44.5±2.9%, 19.3±0.4% and 5.0±0.3% at 0.4, 1 and 4 μL/min flow rates, respectively. In the case of single channel without reservoirs, the conversion was 29.7±1.8%, 13.4±0.7% and 4.1±0.3% at 0.4, 1 and 4 μL/min flow rates, respectively. In the case of cross channel without reservoirs, the conversion was 13.3±0.2%, 6.8±0.3% and 1.5±0.2% at 0.4, 1 and 4 μL/min flow rates, respectively.

Combined, these results demonstrate that by eliminating the reservoirs, the background signal from homogeneous parasitic reactions in the dead volume of interconnects decreases by 33%. By separating the flow directions with the cross channel configuration, the background signals from heterogeneous parasitic reactions on the microchannel walls further decreases by 63%. The total decrease of background signal from the configuration of Fig. 5(a) to that of Fig. 5(c) is 65–70% for the three flow rates tested.

5.2 Enzyme conversion signal/background

To better understand the improvements realized by eliminating interconnect dead volume and separating the flow

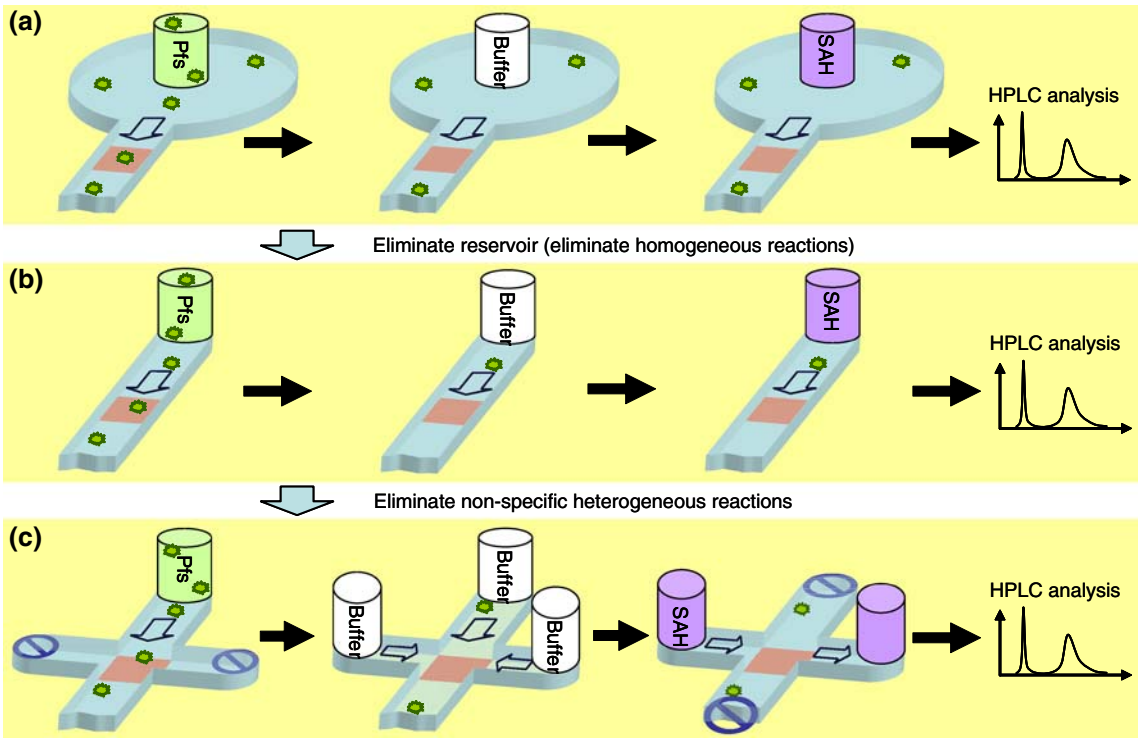

Fig. 5 Minimize parasitic reactions by eliminating interconnect reservoirs and by separating sequential flow directions in cross channels. To test the background signal by parasitic reactions, Pfs enzyme solution was introduced without electro-assembly followed by buffer rinsing, then enzymatic substrate SAH was introduced and products were collected downstream to be analyzed by HPLC. (**a**) Single channel with interconnect reservoirs. (**b**) Single channel without interconnect reservoirs. (**c**) Cross-channel without interconnect reservoirs

(a)

Flow rate (μL/min)	0.4	1	10
1-ch_W/ reservoir	44.5 ± 2.9%	19.3 ± 0.4%	5.0 ± 0.3%
1-cn_No reservoir	29.7 ± 1.8%	13.4 ± 0.7%	4.1 ± 0.3%
X-ch_No reservior	13.3 ± 0.2%	6.8 ± 0.3%	1.5 ± 0.2%

(b)

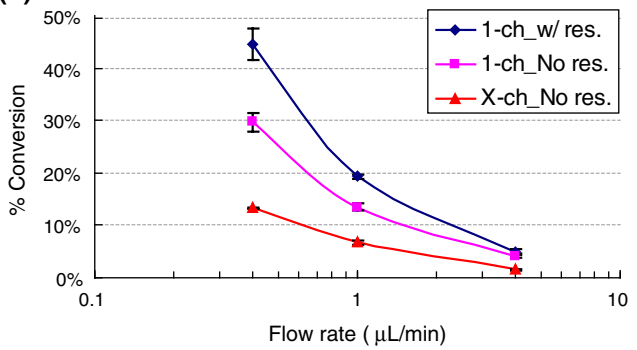

Fig. 6 Background signals (parasitic enzymatic conversion) at different flow rates. Enzyme Pfs solution was introduced without electro-assembly followed by buffer rinsing, then enzymatic substrate SAH was introduced and products were collected downstream to be analyzed by HPLC. Legend: *1-ch_w/ res.* single channel with interconnect reservoirs (*blue*); *1-ch_No res.* single channel without interconnect reservoirs (*pink*); *X-ch_No res.*cross-channel without interconnect reservoirs (*red*)

directions for sequential enzymatic reactions, site-specific heterogeneous enzymatic reactions on the assembly electrode were also performed side by side to compare with the control experiments. The experiments differ from the control experiments only in that an electrical signal of 3 A/m^2 current density was applied to electrodeposit Pfs-chitosan conjugate onto the assembly electrodes during the 4-min incubation of enzyme solution in the channels. The experiments were performed at 0.4 μL/min flow rate for all the three configurations shown in Fig. 5. The enzyme solution for all the experiments and controls was from the same batch, while the conjugate solution was made right before experiments. The background signal was taken from Fig. 6 at the flow rate of 0.4 μL/min.

The experiment results in Fig. 7 show that in the case of the single channel with reservoirs, the site-specific conversion is 32.0±1.6% and the background signal is as high as 44.5±2.9% yielding a signal/background (*S*/*B*) ratio of 0.72. In the case of the single channel without reservoirs design, the site-specific conversion is 38.1±0.6% while the background signal is 29.7±1.8% with the *S*/*B* ratio of 1.28. In the case of the cross channel without reservoirs design, the site-specific conversion is 32.3±3.5% while the background signal is as low as 13.4±0.7% with the *S*/*B* ratio of 2.43. The cross hatched area in Fig. 7 (X-ch_No res) represents calculated missing reaction correction due to a slight reduction in electrode area upon alignment of intersection channels onto electrode (see supplementary section). Note, however, the electrode with only 0.75 mm^2 area represents only 1% of the total microchannel surface (77.15 mm^2), and the volume above the electrode site (0.11 μl) represents only 2.5% of the total microenvironment volume (4.45 μl). Therefore, the conversion on the enzyme-activated electrode is >2 orders of magnitude faster per unit area than the background signal resulting from either parasitic mechanism.

In summary, these results demonstrate that by utilizing our packaging and experimental strategies to minimize the parasitic reactions in interconnect dead volume and by non-specific binding on microchannel walls, we improve the signal-to-background ratio of sequential enzymatic reactions from 0.72 to 2.43.

6 Discussion

Estimation of enzyme specific activity was reported previously (Luo et al. 2008). The enzyme specific activity for the Pfs-chitosan conjugate assembled on the electrode in this paper (0.35 μmol SAH/ min/ mg Pfs) is lower that what we estimated in the previous publication (3.7 μmol SAH min^{-1} mg^{-1} Pfs). The difference might be due to several reasons. Firstly, the enzyme solution used here was from a different batch prepared at different time which might have different specific activity. Secondly, the bioMEMS device used here has a different configuration which might result in different activity after enzyme assembly. The device design in Fig. 3 consists of two counter electrodes besides the working electrode for enzyme assembly. During electrodeposition, this configu-

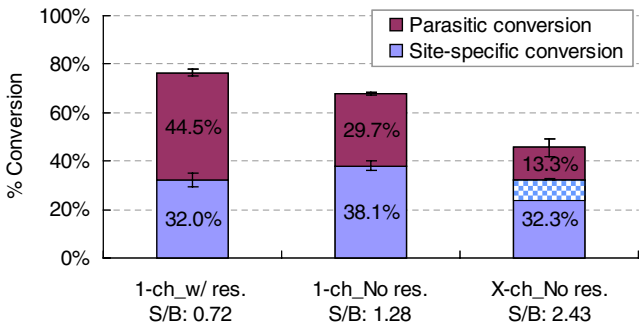

Fig. 7 Conversions by non-specifically bound or trapped enzyme (*blue*) and conversions by site-specifically assembled enzymes (*red*) at 0.4 μL/min flow rate. For the non-specific conversion, no electrical signal was applied to electrodeposit Pfs-chitosan conjugate. For the total conversion, an electrical signal of 3 A/m^2 current density was applied for 4 min to electrodeposit Pfs-chitosan conjugate onto the assembly electrodes. The *cross hatched area* in the case of X-ch_No res represents calculated missing reaction conversion due to a slight reduction in electrode area upon alignment of intersection channels onto electrode (see supplementary section)

ration might generate higher pH gradient at the working electrode surface, thereby deactivating the enzyme activity. Nonetheless, the estimated specific activity is within the range of reported Pfs specific activities in the literature which vary over 3 orders of magnitude (Duerre 1962, Ferro et al. 1976, Ragione et al. 1985). Importantly, given the enzyme specific activity and flow rate conditions, the purpose of suppressing parasitic reactions has been demonstrated by the decreasing background signal and increasing *S*/*B* ratio, as shown in Figs. 6 and 7, while the site-specific conversions remained at the same level.

The use of chitosan as an intermediary interface allows for the programmable assembly of enzymes in a microfluidic network, making this bioMEMS platform both versatile and functional (Fernandes et al. 2004, Wu et al. 2003). By improving the ability to specify the site of the individual enzymatic reactions, these modifications allow for the construction of the complex networks needed to simulate biologically relevant pathways. In these networks, each enzymatic step would be catalyzing a specific reaction with known conversion efficiency. The conversation rate of each step could be measured independently, and the conversion action would be attributable only the specifically bound enzyme, with minimal side-reactions.

Advanced methods for reducing parasitic reactions can be further developed. Homogenous parasitic reactions could be addressed by the use of zero dead-volume interconnect designs to interface the microfluidic channel with the external pumping and fluid delivery. By incorporating in-line valves for flow control, it is possible to envision purging flows which would flush the channel areas of any non-specifically bound enzyme. Additionally, through stronger and longer chemical pretreatment of the microchannel walls than the BSA solution used here, it might be possible to further repel enzyme bounding and thereby eliminate heterogeneous parasitic reactions.

7 Conclusion

In summary, this work demonstrates a novel packaging technique to minimize the homogeneous parasitic reactions in the dead volume of packaging interconnects and an experimental strategy to minimize heterogeneous parasitic reactions due to non-specific binding on microchannel walls. Our experiment and simulation results prove that the combined strategies of fabricating packaging aligners to avoid the interconnect reservoirs and separating flow directions for enzyme immobilization and the subsequent enzymatic reactions are efficient in minimizing the background noise up to 70%. These strategies increase the signal-to-background ratio from 0.72 to 2.43 for the given device design and enzyme activity. These techniques can be easily applied to versatile microfluidic devices to minimize cross-contamination in sequential biochemical reactions.

Acknowledgements This work was supported in part by the Robert W. Deutsch Foundation, the National Science Foundation Emerging Frontiers in Research and Innovation (NSF-EFRI) program under NSF-SC03524414, the Maryland NanoCenter and its FabLab facility.

References

A.A.S. Bhagat, P. Jothimuthu, A. Pais, I. Papautsky, J. Micromech. Microeng **17**, 42–49 (2007) doi:10.1088/0960-1317/17/1/006

U. Bilitewski, M. Genrich, S. Kadow, G. Mersal, Anal. Bioanal. Chem **377**, 556–569 (2003) doi:10.1007/s00216-003-2179-4

A.M. Christensen, D.A. Chang-Yen, B.K. Gale, J. Micromech. Microeng **15**, 928–934 (2005) doi:10.1088/0960-1317/15/5/005

J.A. Duerre, J Biol Chem **237**, 3737–3741 (1962)

R. Fernandes, H.M. Yi, L.Q. Wu, G.W. Rubloff, R. Ghodssi, W.E. Bentley et al., Langmuir **20**, 906–913 (2004) doi:10.1021/la0357312

A.J. Ferro, A. Barrett, S.K. Shapiro, Biochim. Biophys. Acta **438**, 487–494 (1976)

C.K. Fredrickson, Z.H. Fan, Lab Chip **4**, 526–533 (2004) doi:10.1039/b410720a

B.L. Gray, S.D. Collins, R.L. Smith, Sens. Actuators A Phys **112**, 18–24 (2004) doi:10.1016/j.sna.2003.10.073

A. Han, M. Graff, O. Wang, A.B. Frazier, IEEE Sens. J **5**, 82–89 (2005) doi:10.1109/JSEN.2004.838666

D. Janasek, J. Franzke, A. Manz, Nature **442**, 374–380 (2006) doi:10.1038/nature05059

S. Kim, B. Huang, R.N. Zare, Lab Chip **7**, 1663–1665 (2007) doi:10.1039/b713103h

B.S. Ku, J.H. Cha, A. Srinivasan, S.J. Kwon, J.C. Jeong, D.H. Sherman, Biotechnol. Prog **22**, 1102–1107 (2006) doi:10.1021/bp050413+

S.W. Lee, S.S. Lee, Microsyst. Technol.—Micro- and Nanosystems-Information Storage Process. Syst. **14**, 205–208 (2008)

A.T. Lewandowski, D.A. Small, T.H. Chen, G.F. Payne, W.E. Bentley, Biotechnol. Bioeng **93**, 1207–1215 (2006) doi:10.1002/bit.20840

Z. Long, Z. Shen, D. Wu, J. Qin, B. Lin, Lab Chip **7**, 1819–1824 (2007) doi:10.1039/b711741h

X. Luo, A.T. Lewandowski, H. Yi, G.F. Payne, R. Ghodssi, W.E. Bentley, Lab Chip **8**, 420–430 (2008) doi:10.1039/b713756g

J.C. McDonald, G.M. Whitesides, Acc. Chem. Res **35**, 491–499 (2002) doi:10.1021/ar010110q

J.J. Park, X.L. Luo, H.M. Yi, T.M. Valentine, G.F. Payne, W.E. Bentley, Lab Chip **6**, 1315–1321 (2006) doi:10.1039/b603101c

S.R. Quake, A. Scherer, Science **290**, 1536–1540 (2000) doi:10.1126/science.290.5496.1536

E.D. Ragione, M. Porcelli, M. Cartenifarina, V. Zappia, Biochem. J **232**, 335–341 (1985)

Y.C. Tan, V. Cristini, A.P. Lee, Sens. Actuators B Chem **114**, 350–356 (2006) doi:10.1016/j.snb.2005.06.008

T. Thorsen, S.J. Maerkl, S.R. Quake, Science **298**, 580–584 (2002) doi:10.1126/science.1076996

P.L. Urban, D.M. Goodall, N.C. Bruce, Biotechnol. Adv **24**, 42–57 (2006) doi:10.1016/j.biotechadv.2005.06.001

L.Q. Wu, H.M. Yi, S. Li, G.W. Rubloff, W.E. Bentley, R. Ghodssi, Langmuir **19**, 519–524 (2003) doi:10.1021/la026518t

H.M. Yi, L.Q. Wu, W.E. Bentley, R. Ghodssi, G.W. Rubloff, J.N. Culver, Biomacromolecules **6**, 2881–2894 (2005) doi:10.1021/bm050410l